Visual Analysis of Cardiac 4D MRI Blood Flow Using Line Predicates

Silvia Born, Matthias Pfeifle, Michael Markl, Matthias Gutberlet, and Gerik Scheuermann, *Member*, *IEEE*

Abstract—Four-dimensional MRI is an in vivo flow imaging modality that is expected to significantly enhance the understanding of cardiovascular diseases. Among other fields, 4D MRI provides valuable data for the research of cardiac blood flow and with that the development, diagnosis, and treatment of various cardiac pathologies. However, to gain insights from larger research studies or to apply 4D MRI in the clinical routine later on, analysis techniques become necessary that allow to robustly identify important flow characteristics without demanding too much time and expert knowledge. Heart muscle contractions and the particular complexity of the flow in the heart imply further challenges when analyzing cardiac blood flow. Working toward the goal of simplifying the analysis of 4D MRI heart data, we present a visual analysis method using line predicates. With line predicates precalculated integral lines are sorted into bundles with similar flow properties, such as velocity, vorticity, or flow paths. The user can combine the line predicates flexibly and by that carve out interesting flow features helping to gain overview. We applied our analysis technique to 4D MRI data of healthy and pathological hearts and present several flow aspects that could not be shown with current methods. Three 4D MRI experts gave feedback and confirmed the additional benefit of our method for their understanding of cardiac blood flow.

Index Terms—Flow visualization, medical visualization, 4D MRI, line predicates

1 Introduction

A healthy cardiovascular system depends on the effective interplay of blood hemodynamics and the morphology of heart and vessels: On the one hand, the asymmetric and curved shape of the human heart leads to an efficient ejection of blood into the lungs and the body [18]. On the other hand, the flowing blood exerts varying forces on the vascular morphology that causes a necessary and continuous remodeling of the heart and vessel tissue [7]. As a consequence, cardiovascular diseases may develop if this system is destabilized by alterations of blood flow or morphology [7]. That way, the modified morphology causes changes in the blood flow behavior like, e.g., vortices or high-velocity jets. These flow alterations may lead to unfavorable remodeling like, e.g., to aneurysm development. In the long run, serious diseases may result from this vicious cycle.

It becomes obvious that cardiovascular diseases cannot be reduced to morphological aspects. In most cases blood flow aspects are important as well. While imaging of morphology has a long tradition (CT angiography, MR angiography), less regard is paid to patient-specific blood flow information. In clinical routine, flow examinations are usually, if at all, carried out in 2D with either Doppler-Ultrasound or 2D phase-contrast MRI measurements. Flow-sensitive phase-contrast magnetic resonance imaging (4D MRI) closes this gap. It allows us to acquire time-resolved blood flow velocities in 3D over the complete cardiac cycle with a rather good spatial resolution.

However, to exploit the full potential of 4D MRI, appropriate analysis methods are essential. Currently, physicians analyze 4D MRI data mainly by inspecting the flow field or derived flow parameters on manually defined 2D cross-sections. For a 3D impression, the course of streamlines or pathlines started from these 2D planes is examined [2]. Valuable insight in cardiovascular physiology, pathologies, and associated hemodynamics have already been gained with these approaches [21]. However, their drawback is the high degree of user interaction that makes the analysis very time-consuming and the results strongly user-dependent. Further, the current methods fail to provide a good overview of the flow situation. Physicians are not always interested in a confined anatomical area, but want to detect irregular flow behavior somewhere in the heart or vessels. To gain proper overview, several 2D planes need to be selected and examined. This is tedious and the risk of missing crucial aspects is high—especially with complex flow situations as they occur in the human heart.

Recently, we have introduced a visual analysis method that allows the user to interactively investigate the main blood flow behavior in 4D MRI data [4]. Instead of restricting the analysis to local flow patterns and leaving the flow interpretation to the user, this method captures general flow structures. The basic idea is that integral lines represent the spatiotemporal behavior of a flow field. However, inspecting thousands of lines is not helpful for

- *S. Born and G. Scheuermann are with the Department for Computer Science, University of Leipzig, PF 100920, 04009 Leipzig, Germany. E-mail: {silvia.born, scheuermann}@informatik.uni-leipzig.de.*
- *M. Pfeifle is with the Department for Neurosurgery, University Hospital Tübingen, Hoppe-Seyler-Str. 3, 72076 Tübingen, Germany. E-mail: matthias.pfeifle@klinikum.uni-tuebingen.de.*
- *M. Markl is with the Departments of Radiology and Biomedical Engineering, Northwestern University Feinberg School of Medicine, 737 N. Michigan Avenue, Chicago, Illinois 60611. E-mail: mmarkl@northwestern.edu.*
- *M. Gutberlet is with the Department of Diagnostic and Interventional Radiology, Heart Center Leipzig, Strümpellstr. 39, 04289 Leipzig, Germany. E-mail: matthias.gutberlet@herzzentrum-leipzig.de.*

Manuscript received 31 May 2012; revised 31 Aug. 2012; accepted 17 Nov. 2012; published online 29 Nov. 2012.
Recommended for acceptance by H. Hauser, S. Kobourov, and H. Qu.
For information on obtaining reprints of this article, please send e-mail to: tvcg@computer.org, and reference IEEECS Log Number TVCGSI-2012-05-0095.
Digital Object Identifier no. 10.1109/TVCG.2012.318.

understanding the flow. Instead, we allow the user to carve out interesting flow structures by interactively selecting and displaying lines according to relevant flow properties. These properties are, e.g., flow paths, vorticity, velocity, or residence time. For the selection process, we adapted the line predicate approach that was initially introduced for the analysis of nonmedical CFD simulation data [26], [27]. Based on expert input, we defined several line predicates for steady and unsteady blood flow analysis and applied this method successfully to 4D MRI data of the human aorta [4].

Obviously, cardiovascular diseases are not restricted to the aorta or other large vessels, but also affect the heart. Therefore, we present in this paper an adaptation of our visual analysis approach to cardiac 4D MRI blood flow. Cardiac blood flow holds several challenges as shape changes during contraction and the flow, which is more complex (see Section 4.1).

The goal of this work is to provide a line predicate approach, which allows the user to interactively explore heart data. By choosing and combining appropriate predicates, users can bring in their medical knowledge, query the data, and get answers to questions like: "What vortices evolve in the left atrium and how does this change over time?" or "Are there any high-velocity flow jets occurring during the cardiac cycle?".

The establishment of 4D MRI in the clinics is the goal of current research. Still, before this goal can be reached more fundamental research has to be done. For example, to find irregular flow behavior in patient data, it has to be clear what regular behavior is. Further, it has to be clear which flow structures indicate certain pathologies. Hence, at this point we mainly address medical researchers who want to understand the role of cardiac hemodynamics in the development of cardiovascular diseases. Their findings from clinical studies—in addition to appropriate analysis methods—will have a strong impact on the clinical use of 4D MRI.

In summary, these are our main contributions:

- We present a line predicate approach for the visual analysis of 4D MRI data of the heart. This approach takes the heart contractions into account and allows to capture the main blood flow structures according to various properties, such as vortices, flow paths, velocity, and residence time.
- We evaluate our method by presenting feedback of three 4D MRI experts and showing aspects of flow through healthy and pathological human hearts that so far can only be displayed with a lot of effort—if at all.

2 Related Work

Four-dimensional MRI is a rather young imaging modality that has not found its way into the clinical routine yet. Mainly 4D MRI experts have been engaged with the data analysis for research purposes in the last years. Common 4D MRI analysis methods adopted standard flow visualization techniques, such a 3D streamlines or pathlines [3], [5] or the depiction of flow information on 2D planes by means of color-coding, vector plots, or velocity profiles [20]. These methods were enhanced [2], [13], [21] but still demand a lot of interaction and user knowledge to find specific flow patterns in the data.

In recent years, the visualization community discovered 4D MRI blood flow as an exciting research area. There is interest in supporting users by improving the existing methods in terms of usability and comprehensiveness. Van Pelt et al. apply an easier interaction for the selection of 2D vessel cross-sections. Further, they use illustrative methods like arrow-trails to depict time-dependent blood flow dynamics and exploded planar reformats to connect 3D and 2D views of the flow [34]. Gasteiger et al. tackle the problem of occlusion and clutter when vessel morphology and complex flow are visualized together. They introduce a ghosted view approach that displays the vessel surface but reveals the blood flow depending on the orientation between surface and viewer [9]. An approach to encode a multitude of parameters on the 2D plane that separates an aneurysm from the main vessel is presented by Neugebauer et al. [22]. Furthermore, they introduce interaction widgets that are tailored to the needs when examining cerebral aneurysms. A probing approach developed recently by Van Pelt et al. allows to explore flow by interactively injecting seeds into the 4D MRI flow field and observing the flow behavior based on illustrative renderings and animations [32]. A hierarchical clustering method was applied to unsteady 4D blood flow data by Van Pelt et al. to achieve a more sparse flow representation [35]. Angelelli and Hauser [1] developed a method to straighten tubular boundaries to provide a side-by-side visualization helping in comparing tubular flows.

Thus, there exist several promising approaches to improve the depiction of 3D integral lines or flow parameters on 2D planes. A remaining problem, however, is the interpretation of the flow concerning flow patterns and the overall flow behavior that is still mainly left to the user. To assist the user in this task, Heiberg et al. introduced an automatic detection of swirling flow based on a vector pattern matching technique and showed its applicability to 4D MRI data [12]. Krishnan et al. depict particles with similar paths by segmenting integral lines starting from a 2D plane according to their anatomical target area. The clusters are displayed on the emitter planes [19]. Eriksson et al. are concerned with the quantification of blood flow in the left ventricle [7]. They group pathlines based on their start and target regions into several groups (entering, exiting, passing, staying in the ventricle) and determine the volume of the different compartments from this.

Our approach is related to these methods in the sense that we also aim at detecting specific flow behavior. But while the aforementioned methods each deal with one type of flow behavior, we apply a more flexible approach that allows us to structure the flow according to several different properties. To achieve this, we adopt the line predicate approach introduced by Salzbrunn et al. [26], [27] and previously applied to 4D MRI data of the aorta [4]. The pathline attributes by Shi et al. are also closely related to our line predicate approach [28]. They apply linked views to select pathlines with specific parameters in nonmedical data. However, our concept of line selection based on features of the underlying velocity or anatomical data is not readily possible with their technique. In the context of pathline attributes, Pobitzer et al. recently presented an

analysis about the minimal attribute set necessary to adequately represent features for an interactive flow analysis [24]. Interestingly, the identified attributes correlate with the characteristics that we base our line predicates on.

The semantic layers by Rautek et al. [25] are an example for the use of fuzzy-logic to control the illustrative visualization of complex data. Here, data subsets with similar properties are rendered in a similar way. This relates to our approach in the sense that we also control the visualization by selecting flow areas with specific properties and displaying them or not. Thus, we use a binary approach. It is thinkable to also use fuzzy-logic for our application to, e.g., show integral lines fulfilling a property with a certain probability. However, this leads again to a higher number of rendered lines and cluttered visualizations that need to be designed such that they are still comprehensible. As we feel that the medical researchers are more interested in a simple visualization, we aim at an intuitive, uncluttered visualization and prefer the binary predicate evaluation.

Besides 4D MRI blood flow, medical flow visualization plays a role in other medical disciplines as well. Zachow et al. introduced a system for the visual exploration of CFD simulated nasal airflow that provides various information visualization techniques such as parallel coordinates and time series visualizations to examine airflow with respect to velocity, temperature, and humidity [37].

Finally, it needs to be pointed out that the visualization community has tackled cardiac 4D MRI blood flow only superficially so far. This means that analysis techniques developed for blood flow in vessels were only occasionally applied to blood flow in the heart. This work is the first one exclusively addressing cardiac 4D MRI blood flow and its specific challenges.

3 Concepts

In our visual analysis approach, line predicates are used for the selection of flow structures from precalculated streamlines or pathlines. We briefly recapitulate the concepts of integral lines and line predicates [26], [27] in the following sections.

3.1 Integral Lines

The infinite set of integral lines contains all information about the flow dynamics of a given 3D vector field. A *pathline* represents the trace of a virtual particle emitted into an *unsteady* flow field at a specific time and runs tangentially to the velocity vectors. In an unsteady velocity field $v : D \times T \rightarrow \mathbb{R}^3$ (with the field domain $D \subset \mathbb{R}^3$ and time span $T = [t_0, t_n]$), a pathline P is defined as

$$\begin{aligned} P_{a,\tau} : T_{a,\tau} &\rightarrow D \\ P_{a,\tau}(\tau) &= a \\ t &\mapsto P_{a,\tau}(t) \\ \frac{dP_{a,\tau}}{dt}(t) &= v(P_{a,\tau}(t), t), \end{aligned} \tag{1}$$

for starting position $a \in D$, starting time $\tau \in T$ and over time $t \in T$. The time interval $T_{a,\tau} \subset T$ is the maximal lifespan of the particle in D during T.

Streamlines depict the situation in a *steady* flow. Steady flow can be regarded as a special case of unsteady flow where streamlines and pathlines coincide. Accordingly, streamlines are pathlines with time kept fixed ($t = t_i$). Their line parameter is not equivalent to time and therefore depicted by s:

$$\begin{aligned} S_{a,t_i} : B_a &\rightarrow D \\ S_{a,t_i}(0) &= a \\ s &\mapsto S_{a,t_i}(s) \\ \frac{dS_{a,t_i}}{ds}(s) &= v(S_{a,t_i}(s), t_i). \end{aligned} \tag{2}$$

B_a is the maximal integration parameter interval of the streamline in D at $t = t_i$.

Integral lines are equivalent if they describe the path of the same particle or, in the steady case, run through the same position x. The set of all equivalence classes of integral lines is expressed by $\mathcal{P}$.

A 4D MRI heart data set consists of several measurements at different time points altogether covering an averaged cardiac cycle (see Section 4.2). With this data, pathlines represent the movement of blood particles over all measured timesteps, i.e., over the complete cardiac cycle. Streamlines are calculated for a single timestep and capture the blood flow situation at that specific point in time during the cardiac cycle. The course of a streamline is not equivalent to the course of a blood particle through the pumping heart.

3.2 Line Predicates

Predicates are Boolean functions. Thus, a line predicate Λ is a Boolean function, which evaluates to true or false depending on whether a considered integral line $P_{a,\tau} \in \mathcal{P}$ meets a certain characteristic

$$\begin{aligned} \Lambda : \mathcal{P} &\rightarrow \{\text{true}, \text{false}\} \\ P_{a,\tau} &\mapsto \Lambda(P_{a,\tau}). \end{aligned} \tag{3}$$

The characteristic set $\mathcal{C}_\Lambda$ of a line predicate Λ defines all points in spacetime visited by lines fulfilling this predicate

$$\mathcal{C}_\Lambda = \{\ (x,t) \in D\ \times T \mid \Lambda(P_{x,t}) = true\},$$

with $t = t_i$ for the characteristic sets of streamline predicates (see Section 3.1).

3.3 Line-Based and Derived Predicates

Line-based and derived line predicates differ in the data that is used for their evaluation: For *line-based* predicates the examined feature depends only on characteristics of the integral line itself; *derived* predicates deal with features of the corresponding velocity field or anatomical volume data set. The detection of a derived feature is equivalent to the evaluation of a point predicate Γ that evaluates to true, if a feature is present at a point in spacetime

$$\begin{aligned} \Gamma : D \times T &\rightarrow \{\text{true}, \text{false}\} \\ (x,t) &\mapsto \Gamma(x,t). \end{aligned} \tag{4}$$

The result of the point predicate is then used as input for the derived line predicate. The line predicate resolves to *true*, if a pathline $P_{a,\tau}$ is present at $(x,t) \in D \times T$ where $\Gamma(x,t) = true$:

$$\Lambda(P_{a,\tau}) = \begin{cases} true, & \text{if } \exists t \in T_{a,\tau},\ P_{a,\tau}(t) = x \\ & \text{and } \Gamma(x,t) = true, \\ false, & \text{otherwise.} \end{cases} \quad (5)$$

In the steady case, for streamline S_{a,t_i}:

$$\Lambda(S_{a,t_i}) = \begin{cases} true, & \text{if } \exists s \in B_a,\ S_{a,t_i}(s) = x \\ & \text{and } \Gamma(x,t_i) = true, \\ false, & \text{otherwise.} \end{cases} \quad (6)$$

4 Cardiac Blood Flow Analysis

We present a method using line predicates for the analysis of 4D MRI cardiac blood flow data. The basic idea of our line predicate approach is that the full set of integral lines contains all necessary information about a data set's blood flow dynamics. Visualizing flow with streamlines and pathlines is very intuitive, but displaying too many lines at a time is confusing and hinders insight. In our approach, we, therefore, allow the user to interactively select and display lines of interest (e.g., with a certain velocity, running through a certain anatomical area or the like). For this selection process, we provide the user with several line predicates. These predicates were formulated based on the input of 4D MRI experts. Together with an automatic vortex detection, this forms a tool box that helps the user to explore the 4D MRI data and easily display distinct flow structures of interest. With this approach, we give an alternative to current analysis techniques, which also use integral lines but leave the flow interpretation fully to the user.

In the following, we describe the blood flow through the human heart and the resulting challenges.

4.1 Blood Flow in the Human Heart

The human heart pumps oxygenated blood from the lungs into the body (aorta). This is done via the *left heart*. Further, the heart pumps deoxygenated blood from the body back into the lungs for oxygenation (pulmonary artery). This happens in the *right heart*. The left and the right heart are usually completely separate flow paths.

Both hearts are divided into two chambers—the right and left atrium and the right and left ventricle. The blood enters the heart through the atria (see Fig. 1(left)), flows into the ventricles when the connecting valves open and the atria contract (*diastole*, see Fig. 1(middle)). Finally, the blood is ejected into the aorta or the pulmonary artery respectively when the ventricles contract (see Fig. 1(right)). The atrial filling and ventricular ejection happen almost simultaneously (*systole*). The analysis of cardiac blood flow is challenging for several reasons:

- The heart muscle contracts during the cardiac cycle. Thus, the field domain D is not constant over time. This needs to be handled during data preprocessing (segmentation, integral line calculation) and the evaluation of derived line predicates.
- Irrespective of the contractions, the heart geometry with its four chambers makes the blood flow itself more complex than, e.g., the blood flow in large vessels.
- The data quality of a 4D MRI data set capturing the whole heart is lower compared to an aorta data set. To achieve a tradeoff between acquisition time and size of the captured anatomical area, the data's spatial resolution is decreased. Related to this and because the heart valves between chambers are very thin, the integral lines do not fully obey these anatomical borders (partial volume effect).

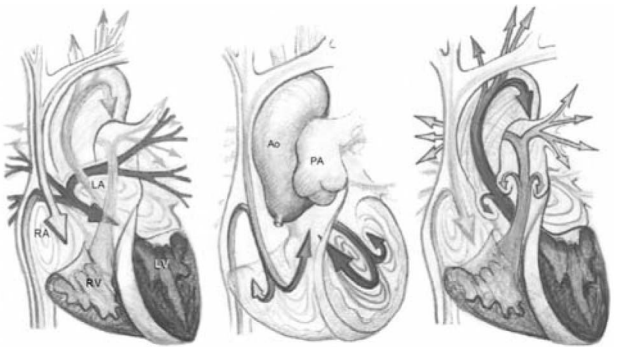

Fig. 1. Schematic drawing of the cardiac blood flow showing the atrial filling (left), the ventricular filling (middle), and the ventricular ejection (right). The flow path through the left and right heart is depicted with dark and light arrows respectively. Abbreviations: Ao, aorta; LA, left atrium; LV, left ventricle; PA, pulmonary artery; RA, right atrium; RV, right ventricle. Reprinted by permission from Macmillan Publishers Ltd: Nature 404: Kilner et al. [18], © 2000.

These challenges need to be handled during preprocessing and line predicate evaluation. In Sections 4.3 and 4.4, we introduce line predicates for the analysis of 4D MRI cardiac blood flow. In the following section, we explain the complete workflow and the necessary preprocessing of the 4D MRI heart data.

4.2 Workflow and Data Preprocessing

With 4D MRI, an anatomical data set and three velocity data sets are acquired simultaneously (see Fig. 2(left)). From the three velocity data sets—each representing the flow velocity in one of the three spatial directions—a velocity vector field is derived. A 4D MRI data set covers an averaged cardiac cycle with a temporal resolution of about $40\,\mathrm{ms}$. This corresponds to 16-24 separate timesteps. The spatial resolution of 4D MRI heart data is in the range of $3.0 \cdot 3.0 \cdot 3.0\,\mathrm{mm}^3$ per voxel. More details on the data used in this paper are given in Section 5.

Our line predicate approach is divided into two main phases. As depicted in Fig. 2, a data preprocessing phase is required to segment the heart, calculate the integral lines, and detect vortices. Then, the visual analysis can take place where the user can freely combine line predicates to explore the flow data. In the following, we explain the needed preprocessing steps.

4.2.1 Segmentation

As a first step, the heart anatomy of interest needs to be segmented. This may be the left or the right heart or both, each consisting of atrium, ventricle, and adjacent vessels, varying significantly during the cardiac cycle. The segmentation is used later on as seed masks for the line tracking, as predefined anatomical regions of interest for several derived predicates, and as context for the line visualization. During segmentation, each timestep needs to be handled separately to ensure that at every point in time the integral lines cover the complete area of interest and the predefined

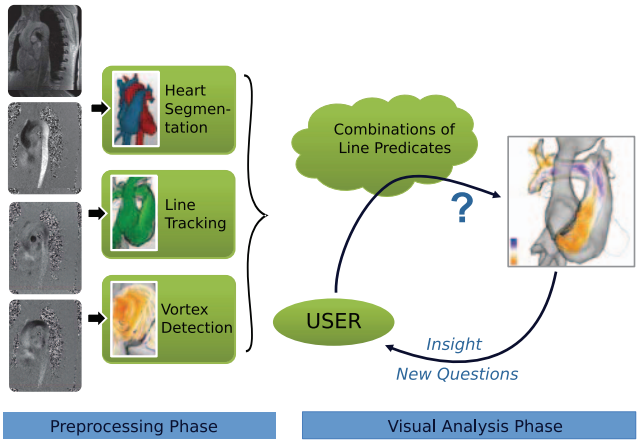

Fig. 2. Workflow: In the data preprocessing step, the anatomical (left, top image) and the velocity data sets (left, lower three images) are used to segment the heart, precalculate integral lines, and detect vortices. In the visual analysis phase, the precalculated information is used to provide the user with a line predicate tool box for an easy exploration of the 4D MRI data set.

regions-of-interest (ROI) correlate with the desired anatomical area.

An initial segmentation mask is created based on the average velocity values reached at each voxel over the cardiac cycle. As heart chambers and vessels have higher average velocities than areas without blood flow, a region-growing can be used to segment the maximally expanded heart chambers and vessels. With the use of anatomical information and the absolute velocity values at every timestep, this initial mask is manually adapted for each timestep to comply with the current shape of atria and ventricles.

With this manual segmentation approach, we can show the feasibility of our method. However, as this requires a significant preprocessing overhead, an advanced segmentation technique is necessary for larger amounts of data or the clinical routine. For a more automated heart segmentation, it is thinkable to, e.g., utilize a level set method as it is already used for 4D MRI heart data [16] or a deformable model approach as it was presented for the segmentation of large vessels [33].

4.2.2 Integral Line Precalculation

The previously generated segmentation masks are used as seeding masks for line integration. Pathlines are generated with a DOPRI5 integration [6]. We require that every temporal flow pattern larger than twice the voxel size is captured by the pathlines. This implies that at least one particle is present in each voxel at each timestep. The straight-forward approach of seeding a particle in each voxel at each timestep results in a large number of lines containing a lot of redundant flow information. To speed up the method, we reduce the number of seeded lines (based on the method in [27]): For the first timestep, particles are seeded in each voxel of this timestep's seeding mask. For the second timestep, particles are emitted only in voxels of the second timestep's seeding mask, which are unvisited by previous particles at that point in time. This procedure is repeated for all timesteps until all voxels are visited in each timestep. Compared to the trivial approach, this reduces the number of lines by 81-95 percent. Streamline calculation is carried out analogously providing that at least one streamline runs through each voxel of the corresponding segmentation mask.

Both, streamlines and pathlines, are then stored as line strips, together with the current velocity and the line parameter value for each vertex x_i. Further, for the evaluation of line-based predicates (see Section 4.3) several other line-based parameters like line length len, maximal velocity v_{max}, and mean velocity $\bar{v}$, are calculated for each integral line. Finally, we precalculate a lookup table that assigns to every voxel in the field domain D all integral lines crossing them and, for pathlines, at what point in time. Derived predicates (see Section 3.3) are evaluated by determining all lines running through a specific set of voxels. The cost for this test when implemented straightforwardly, i.e., by testing every line vertex whether it lies within a volume of interest, depends on the number of lines, line vertices, and voxels. We reduce the costs for this test significantly with the lookup table. Since a quick predicate evaluation is essential for an interactively usable visual analysis tool, we accept the resulting memory overhead.

4.2.3 Vortex Detection

Since our approach is meant to help identify important flow structures, we provide an automatic vortex detection. The vortex core line detection by Sujudi and Haimes [31] and the λ_2 vortex region detection by Jeong and Hussain [14] belong to the standard methods in CFD simulation data (cf. [15] for a detailed survey). These vortex detection methods can be restated to point predicates that determine for each voxel at a specific point in time whether a vortex or a vortex core line respectively is present at this position or not [27]. The point predicate for the λ_2 method [14] is expressed by

$$\Gamma_{\lambda_2}(x,t) = \begin{cases} true, & \text{if } S^2+\Omega^2 \text{ at position } x \\ & \text{and time } t \text{ has 2} \\ & \text{negative eigenvalues,} \\ false, & \text{otherwise.} \end{cases} \quad (7)$$

$S = \frac{1}{2}(J + J^T)$ and $\Omega = \frac{1}{2}(J - J^T)$ are the symmetric and asymmetric parts of the vector field's Jacobian matrix J.

The vortex core line detection by Sujudi and Haimes [31] formulated with the parallel vectors operator by Peikert and Roth [23] results in the following point predicate:

$$\Gamma_{SH}(x,t) = \begin{cases} true, & \text{if at time } t,\ J(x,t) \text{ has complex} \\ & \text{eigenvalues and} \\ & \mathbf{v}(x,t) \parallel (J(x,t)\mathbf{v}(x,t)), \\ false, & \text{otherwise.} \end{cases} \quad (8)$$

$J(x,t)$ is the Jacobian matrix entry for position x at time t. Since 4D MRI data contains more noise than simulation data, it is most likely that a vortex detection method produces false positives. Therefore, we combine the previously described techniques: On the one hand, we detect vortex core lines and discard lines shorter than 30 mm. On the other hand, we apply the λ_2-method. Finally, we define a vortex as detected if at a voxel a core line is present and the λ_2 point predicate returns true (see Figs. 3a and 3b).

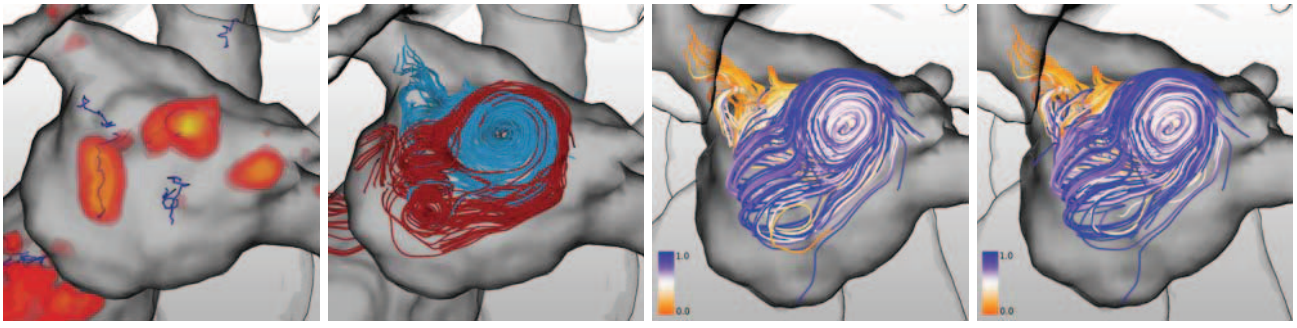

Fig. 3. (a,b) A vortex is detected if both the λ_2 and the Sujudi-Haimes method yield a positive result. (a) Detected vortex core lines and the λ_2-result in the left atrium of a healthy heart for $t = 672$ ms. The volume rendering depicts λ_2 values from $-8.0 \cdot 10^{-5}$ (red) to $-2.5 \cdot 10^{-3}$ (yellow). (b) Streamlines running through the vortex regions that were previously detected both by λ_2 and Sujudi-Haimes. (c,d) The results of a vortex predicate evaluated based on λ_2 (c) and based on a voxelized vortex core line (d) are almost identical. The depicted vortex is located in the left atrium of a healthy volunteer during diastole (at $t = 672$ ms).

With this, the vortex core line is detected. The vortex region can be determined based on the λ_2-result. In practice, however, this depends on a well-chosen threshold, as 0 does not always give usable results, especially with measured data. 4D MRI heart data has a rather low spatial resolution. Thus, we use the original voxel representation of the vortex core line as approximation of the vortex region. A comparison of this approach with the use of the λ_2-result shows that the results of the vortex predicates do not differ significantly (see Figs. 3c, and 3d). However, further research is needed on this topic as for very small or very large vortices the regions might be overestimated or underestimated, respectively. Also, we achieved robust results by discarding all vortex core lines shorter than 30 mm. A higher threshold increases the risk of missing important vortices and a lower threshold increases the risk of false positives. Still, it should be investigated whether this threshold could be more flexibly adapted to the current data set.

For the actual evaluation of vortex predicates later on, a ROI point predicate Γ_{ROI} is used to test whether a point (x, t) in spacetime is part of a vortex region I_{vor}.

4.3 Analysis of Steady Blood Flow

The following line predicates allow the exploration of steady blood flow, i.e., they can be applied to streamlines of a single measured timestep of the 4D MRI heart data. Thus, with these line predicates one cannot yet draw conclusions about the spatiotemporal flow behavior of the blood through the heart, but about the flow situation at a specific point in time during the cardiac cycle.

4.3.1 ROI Predicate

An apparent interest about the cardiac blood flow is the course the blood takes through the different chambers. With the ROI line predicate Λ_{ROI} streamlines can be selected based on anatomical regions they run through. These anatomical regions change in shape and position over the cardiac cycle due to the heart contractions. Thus, a ROI I is a subset of $D \times T$, i.e., it is part of the field domain D and can vary over time.

The ROI point predicate Γ_{ROI} determines whether a point x is part of a ROI I at time t:

$$\Gamma_{ROI}(I, x, t) = \begin{cases} true, & \text{if } (x, t) \in I, \\ false, & \text{otherwise.} \end{cases} \tag{9}$$

The user can either interactively define a ROI or select one from the predefined regions, such as the different chambers, the areas of the valves and the adjacent vessels. The ROI line predicate Λ_{ROI} evaluates to true, if the course of a respective streamline intersects at least one voxel of this specified area I:

$$\Lambda_{ROI}(S_{a,t_i}, I) = \begin{cases} true, & \text{if } \exists s \in B_a, \\ & S_{a,t_i}(s) = x \text{ and} \\ & \Gamma_{ROI}(I, x, t_i) = true, \\ false, & \text{otherwise.} \end{cases} \tag{10}$$

By combining several ROI predicates one can select lines even more specifically and display, e.g., streamlines entering the left atrium but not continuing into the left ventricle. The latter is possible because one can also use negative predicates and select lines *not* running through a specific area. A special version of the ROI predicate determines whether the beginning of the line is inside the ROI. This helps to select lines starting at a specific anatomical area.

4.3.2 Vortex Predicate

Vortices are of special interest for blood flow analysis. Vortices emerging, e.g., in the healthy human aorta or the left ventricle are rather well understood [8], [17]. The occurrence of abnormal vortices may, therefore, be an indication for a pathology and significant for disease prognosis.

With the vortex predicate, streamlines running through a specific vortex can be determined. This way, not only the vortex region itself, but the flow area influenced by the vortex, can be identified. A prerequisite for this predicate is the detection of vortices in the underlying vector field (see Section 4.2). Based on this, the vortex predicate Λ_{vor} evaluates to true, if the streamline traverses a voxel of the respective vortex area I_{vor}. Thus, Λ_{vor} is defined analog to (10). An example for streamlines selected with the vortex predicate is shown in Fig. 3d.

4.3.3 Maximal Velocity Predicate

This predicate identifies streamlines with a maximal velocity v_{max} in a specified interval $[v_1, v_2]$. With $[v_1, \infty]$, e.g., this allows the physician to identify areas with high velocities that usually correspond to the main flow paths. As an example, this predicate allows to easily capture the flow during systole when blood is ejected from the ventricles. Also, these flow paths can form a significant criterion during diagnostics as high-velocity jets may also indicate pathologies like valvular stenosis.

The maximal velocity predicate $\Lambda_{v_{max}}$ is line-based, i.e., it is evaluated according to the precalculated parameter v_{max} (see Section 4.2) for each streamline S_{a,t_i}:

$$\Lambda_{v_{max}}(S_{a,t_i}, v_1, v_2) = \begin{cases} true, & \text{if } v_{max}(S_{a,t_i}) \in [v_1, v_2], \\ false, & \text{otherwise.} \end{cases} \quad (11)$$

4.3.4 Mean Velocity Predicate

Along the lines of the previous predicate, this function identifies integral lines with a mean velocity in a specific interval $[v_1, v_2]$. As a result, areas with a high average velocity can be distinguished from areas with low average speed. The respective predicate $\Lambda_{\bar{v}}$ is defined analog to (11) and evaluated based on the precalculated mean velocity $\bar{v}$ of each streamline (see Section 4.2).

4.3.5 Regional Velocity Predicate

Due to noise or partial volume effects, it occurs that integral lines cross anatomical borders, such as closed valves. Thus, flow areas are wrongly connected and cannot be analyzed separately. One arising problem is that the selection of integral lines with a specific velocity in a specific region gets difficult. Applying a maximal velocity predicate might select unwanted lines as, e.g., the blood flow in the neighboring heart chamber is faster and masks the desired lines. A combination with a ROI line predicate (removing the lines in the neighboring chamber) also eliminates lines of interest. To solve this problem, we define the regional velocity predicate that evaluates to true if a line reaches a velocity $v \in [v_1, v_2]$ in a defined anatomical region I:

$$\Lambda_{v_r}(S_{a,t_i}, I, v_1, v_2) = \begin{cases} true, & \text{if } \exists \sigma \in B_a, \\ & \frac{dS_{a,t_i}}{ds}(\sigma) \in [v_1, v_2], \\ & S_{a,t_i}(\sigma) = x \text{ and} \\ & \Gamma_{ROI}(I, x, t_i) = true, \\ false, & \text{otherwise.} \end{cases} \quad (12)$$

4.3.6 Length Predicate

The length predicate Λ_{len} allows to structure the flow according to streamline length and allows to, e.g., filter out shorter lines that oftentimes lead to clutter. It identifies lines with a length in the interval $[l_1, l_2]$ and is defined analogously to (11).

4.4 Analysis of Unsteady Blood Flow

While the steady analysis of a single timestep of the 4D MRI data allows to explore flow patterns at a fixed point in time, the unsteady analysis allows to capture features of the flowing blood over time. As the steady flow is a special case of the unsteady flow, the majority of the previously explained predicates can be applied here as well: The line-based predicates concerned with mean velocity, maximal velocity, and line length can be adopted without change. With respect to the derived line predicates, the regional velocity predicate and the ROI line predicate as explained in Section 4.3 can be used in the unsteady case. Since the ROI point predicate Γ_{ROI} is time-dependent, the varying shapes of the respective anatomical areas are considered. Thus, the ROI line predicate determines pathlines intersecting a ROI at *any* time during the cardiac cycle. An additional time-dependent ROI line predicate is introduced in the following to select pathlines running through an area at a *specific* point in time. The vortex predicate cannot be used as is. A necessary time-dependent variant is explained shortly. Finally, a residence time predicate is introduced that allows to display pathlines residing in a ROI for longer than a user-defined time interval.

4.4.1 Time-Dependent ROI Predicate

When inspecting the course of pathlines, one might be interested in pathlines that flow through a specific area at a certain time t_i to, e.g., examine their subsequent course by applying further predicates. As in the steady case, the ROI is either selected from the predefined ROIs or defined manually by the user. Then, the ROI predicate Γ_{tROI} determines all pathlines flowing through this area at the given time t_i.

$$\Lambda_{tROI}(P_{a,\tau}, I, t_i) = \begin{cases} true, & \text{if } P_{a,\tau}(t_i) = x \text{ and} \\ & \Gamma_{ROI}(I, x, t_i) = true, \\ false, & \text{otherwise.} \end{cases} \quad (13)$$

4.4.2 Time-Dependent Vortex Predicate

In an unsteady flow field, the location and shape of vortices change over time. Therefore, the vortices are detected for each timestep and the pathlines are queried for whether they flow through the respective area at a specific time t_i:

$$\Lambda_{tVor}(P_{a,\tau}, I_{vor}, t_i) = \begin{cases} true, & \text{if } P_{a,\tau}(t) = x \text{ and} \\ & \Gamma_{vor}(I_{vor}, x, t_i) = true, \\ false, & \text{otherwise.} \end{cases} \quad (14)$$

Inspecting the influence of a vortex on a pathline over a longer time is accomplished by combining vortex predicates for subsequent timesteps. Tracking a vortex over several timesteps can be accomplished geometrically, similar to the volume tracking method of Silver and Wang [30]. This approach is feasible, as the main vortices occurring in heart chambers are rather large compared to the chamber size and do not dislocate significantly over time (see Fig. 5). Further, in case vortices are wrongly identified as being the same vortex in different timesteps, the time-dependent vortex predicate will not show meaningful results with this input. Therefore, the predicate evaluation can be seen as proof that the vortex mapping is correct.

4.4.3 Residence Time Predicate

This pathline predicate determines whether a particle spends longer than a specified time span $t_r > 0$ in a predefined ROI. The residence time of particles in the heart can be used as a measure for the efficiency of the working

heart. Further, long residence times of particles in, e.g., a vortex region, indicate a higher risk for thrombogenesis and, thus, of suffering from stroke or a heart attack. The residence time predicate Λ_{res} can be expressed with

$$\Lambda_{res}(P_{a,\tau}, I, t_r) = \begin{cases} true, & \text{if } \exists t_1, \exists t_2,\ (t_2 - t_1) \geq t_r, \\ & \forall t \in [t_1, t_2], \\ & \Lambda_{tROI}(P_{a,\tau}, I, t) = true, \\ false, & \text{otherwise.} \end{cases} \tag{15}$$

As with the steady blood flow analysis, the previously described predicates can be freely combined. When defining the flow structure with a set of predicates, it is important to make sure that the resulting characteristic sets are disjoint (see Section 3.2).

4.5 Flow Structure Visualization

The lines selected by the different predicates are visualized in the context of the corresponding heart mesh and the anatomical MRI slice data (optionally). With the rendering of the heart chamber models, we differentiate between focus and context rendering: The context rendering consists of silhouette renderings together with an illustrative shading technique (halftoning). The focus rendering displays the background (backfacing polygons) of the chambers as gray isosurfaces. The front layer (front-facing polygons) is rendered illustratively like the context models. The focus rendering is used for the chambers for which the respective lines are currently examined. The context rendering is used for the remaining chambers because it is an unobtrusive way of giving some anatomical orientation. Usually, one investigates the blood flow either through the left or the right heart. This means that oftentimes the left heart is rendered as focus and the right heart as context or vice versa.

The integral lines are rendered as color-coded tubes. The color-coding either represents the complete line's mean velocity or the changes of parameters along the course of the line. In the latter case, the colors represents the velocity or the line parameter at the individual line vertices. The line parameter encoding gives information about the flow direction in case this may not be clear from the context. Despite of the perceptual disadvantages of the rainbow color map, it is still the common way of depicting line parameters in medical software and publications. Not following this convention, but the advice of Silva et al. [29], we decided on using diverging maps. Due to feedback of users who suggested using different colormaps for different parameters, we apply colormap ranging from orange (small values) to purple (large values) for the line parameter and a colormap ranging from green (small values) to pink (large values) for the velocity.

To show the course of lines over time, it is also possible to display not the complete line but only segments according to the line parameters (see Fig. 5).

We implemented the line predicate approach as a scene graph addition to our medical visualization framework. The predicates are represented by separate scene graph nodes that can be combined freely during runtime. Except for the user-defined predicate parameters (e.g., velocity of interest), no parameter adjustment is necessary.

5 Application and Evaluation

Two 4D MRI data sets were analyzed with our method and three 4D MRI experts gave feedback during the analysis. In the following sections, we introduce the used data sets and present the data-specific insights gained from the analysis. Finally, we summarize the general expert feedback that we received during data analysis.

5.1 Data

We applied our method to two 4D MRI data sets of the human heart. One data set shows a healthy heart, one shows a pathological heart several years after surgical repair of a tetralogy of Fallot. Tetralogy of Fallot (TOF) is a congenital heart defect involving a hole in the septum between the ventricles and a narrowing of the right ventricular outflow tract or pulmonary valve or both, as well as right ventricular hypertrophy and an overriding aorta. During surgery very early in life, the septum hole is closed and the narrowing is, in this case, treated by removing muscle tissue around the pulmonary outflow tract and integrating a transannular patch. As a result, this patient has a pulmonary valve incompetence of a certain degree, which usually increases with growth.

Both data sets were acquired with a temporal resolution of $38.4\ \mathrm{ms}$ and a velocity sensitivity (maximal velocity that can be measured) of $150\ \frac{\mathrm{cm}}{\mathrm{s}}$. The healthy data set has a spatial resolution of $3.0 \times 3.0 \times 3.0\ [\mathrm{mm}^3]$ and covers a heart cycle of $920\ \mathrm{ms}$ in 24 timesteps. The pathological data set has a spatial resolution of $2.5 \times 2.5 \times 3.6\ [\mathrm{mm}^3]$ and covers a heart cycle of $595.2\ \mathrm{ms}$ in 16 timesteps.

To handle image artifacts common for 4D MRI data (noise, eddy-currents), the data sets have already been preprocessed with methods based on Walker et al. [36]. After that, heart segmentation and ROI definition, precalculation of integral lines, and vortex detection is accomplished as described previously in Section 4.2. For a typical 4D MRI heart data set, the preprocessing phase takes around 1.8 hours. The additional overhead for the manual segmentation depends strongly on the anatomical knowledge of the user and may last up to 8 hours. For a potential use in the clinical or research routine, this time needs to be reduced by using advanced segmentation techniques and accelerating the line integration, e.g., by using the GPU.

5.2 Application to 4D MRI Heart Data

A complete discussion of the data sets is clearly beyond the scope of this paper. Thus, we selected a few important aspects to illustrate the benefit of our method.

TOF is known to involve a strong retrograde flow from the pulmonary trunk due to the pulmonary valve incompetence back into the right ventricle during diastole as well as an imbalanced flow into the right and left lung [10], [11]. These two aspects can be very well visualized with our line predicate approach and become especially evident in comparison with the healthy cardiac flow situation.

5.2.1 Flow to Left and Right Lung

Fig. 4a depicts systolic blood flow in a healthy heart from the right ventricle into the pulmonary arteries. The streamlines are selected with the maximal velocity predicate

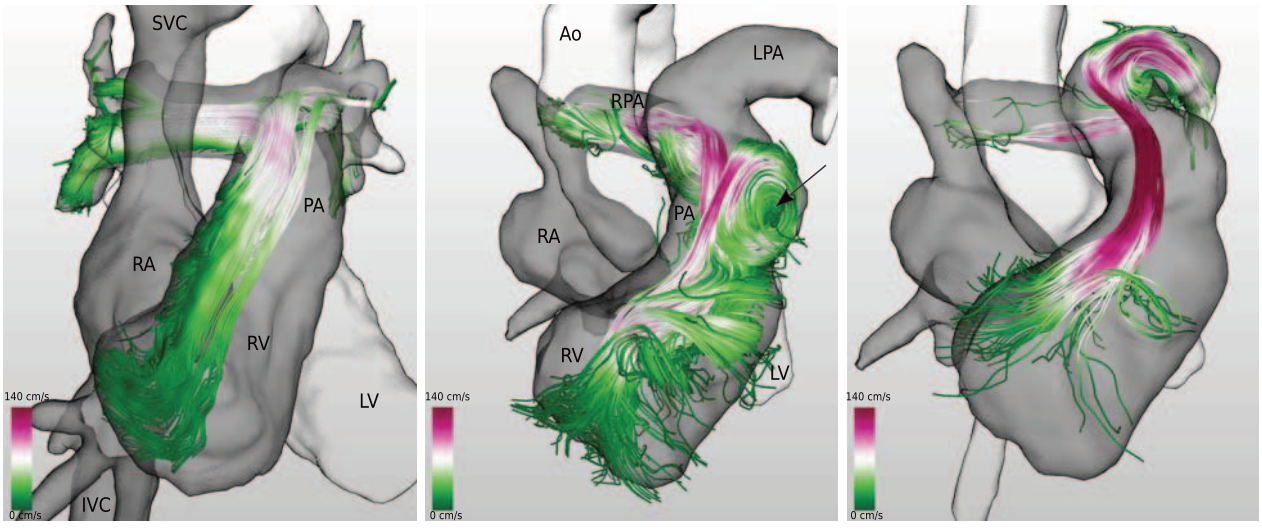

Fig. 4. Flow ratio into left and right lung during systole. Color-coding represents velocity. (a) Fastest streamlines in the pulmonary outflow tract of a healthy heart ($v_{max} > 90\ \frac{\text{cm}}{\text{s}}$). (b) Flow through upper detected vortex (arrow) directed at the RPA. (c) High-velocity jet ($v_{max} > 165\ \frac{\text{cm}}{\text{s}}$) directed at the LPA. Abbreviations: RA, right atrium; RV, right ventricle; LPA, left pulmonary artery; RPA, right pulmonary artery.

($v_{max} > 90\ \frac{\text{cm}}{\text{s}}$). The systolic blood flow shows no vortices and is almost evenly distributed to the left and right pulmonary artery.

The pulmonary trunk of the TOF patient, however, shows bulges that have developed since surgery. Vortex detection shows large vortices in these bulges over the majority of the cardiac cycle. In Fig. 4b streamlines running through the vortex detected in the upper bulge during systole are depicted. It stands out that this vortex strongly correlates with the vortex below and that all streamlines are directed toward the right pulmonary artery. Further, a cavity in the line bundle can be noticed. Applying a maximal velocity predicate to the same streamlines shows a strong high-velocity jet ($v_{max} > 165\ \frac{\text{cm}}{\text{s}}$) running through the cavity of the previous bundle into the left pulmonary artery (see Fig. 4c). Thus, with only these two predicates, one can observe that the right pulmonary artery is affected by the slower vortical flow whereas the left pulmonary artery is directly supplied with fast-flowing blood. With current techniques, the high-velocity jet, flow ratio to the left and right pulmonary artery and, to a certain extent, the large vortices can be determined, but a causal relationship between these flow features cannot be easily observed. Our findings, however, suggest that, in addition to other anatomical changes due to the surgical manipulation, one cause for the imbalanced flow ratio into left and right lung are the large vortices in the bulges. They slow down the flow to the right lung and increase the blood velocity to the left lung. Further, the detected vortices at the beginning of the pulmonary trunk may indicate that the tissue in these areas will further dilate and another surgery will become necessary in the future.

5.2.2 Retrograde Flow

Fig. 5a shows pathlines in the healthy heart flowing from the right atrium into the right ventricle at any time during the cardiac cycle, i.e., two ROI line predicates for atrium and ventricle are combined. From this image, one can get a vast impression of the unsteady blood flow. In Figs. 5b, 5c, 5d, and 5e, an additional vortex predicate can be used to reduce the number of lines. Here, pathlines are selected with a time-dependent vortex predicate that run through a vortex

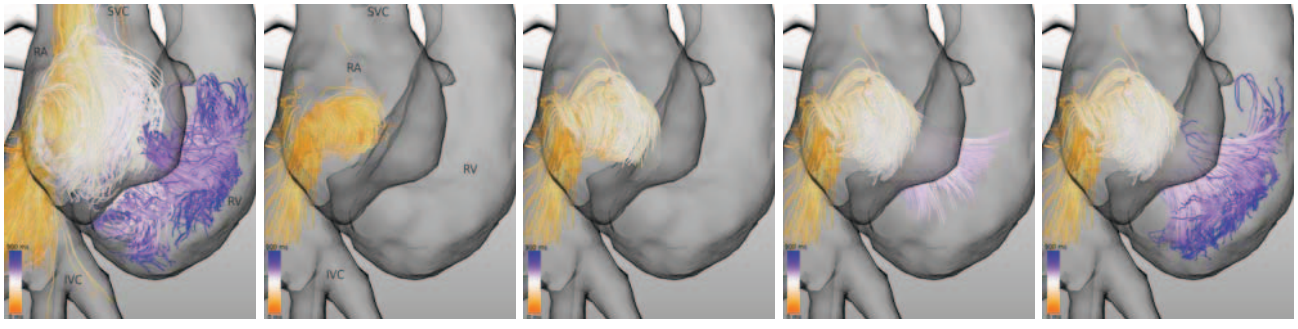

Fig. 5. Pathlines in the healthy heart. Color-coding represents time. (a) All pathlines running through right atrium and right ventricle with $l > 20\ \text{cm}$. (b)-(e) Pathlines running through large vortex in the atrium at $t = 403\ \text{ms}$. Pathlines are shown from beginning of the cardiac cycle until (b) $t = 211\ \text{ms}$ (c) $t = 326\ \text{ms}$ (d) $t = 556\ \text{ms}$ (e) the end of the cycle. The pictures show the transformation of the large vortex in the right atrium into a helical inflow into the right ventricle. Abbreviations: RA, right atrium; RV, right ventricle; SVC, superior vena cava; IVC, inferior vena cava.

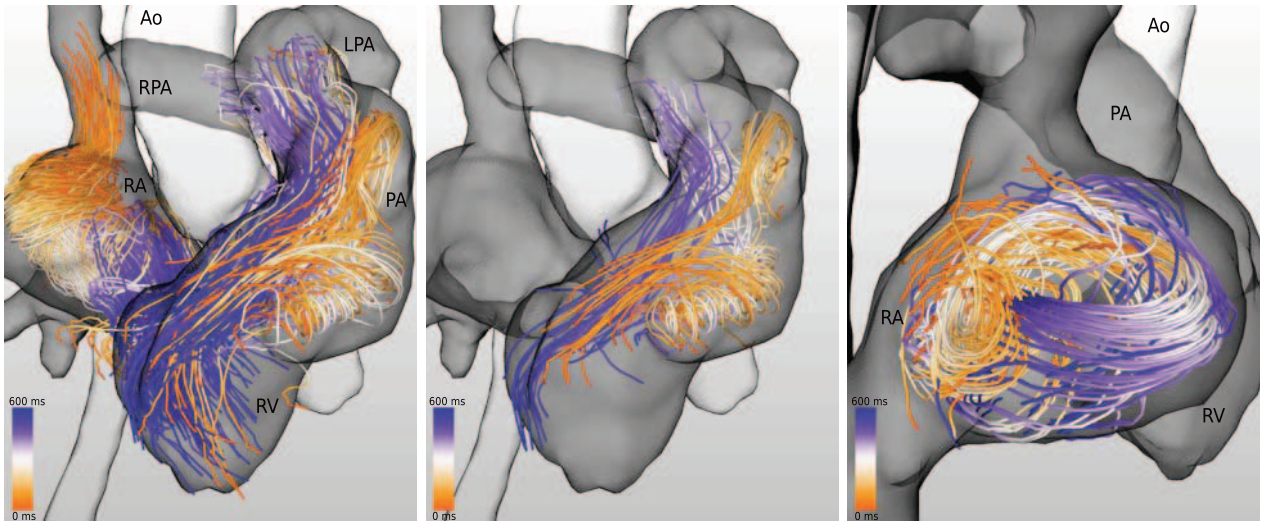

Fig. 6. Retrograde flow in the TOF data set. Color-coding represents time. (a) In diastole the right ventricle receives blood from the right atrium and via retrograde flow from the pulmonary trunk. (b) Pathlines running through vortices during systole and returning to the right ventricle in diastole. (c) Higher residence times $t_r = 550\ \mathrm{ms}$ can be observed in the right atrium of the TOF data set. Abbreviations see Fig. 4.

detected in the right atrium at $t = 403\ \mathrm{ms}$. Figs. 5b and 5c show that these particles enter the atrium mainly through the inferior vena cava and start rotating in the vortex. As the valves open (see Fig. 5d), the vortex transforms into a helical inflow into the right ventricle that starts to form a circular vortex, assumedly as the particles hit the opposite wall of the ventricle (see Fig. 5e). Note that in a healthy heart, this is the only way that blood enters the right ventricle. There is no retrograde flow from the pulmonary trunk.

Fig. 6 shows the respective flow situation in the TOF patient. A time-dependent ROI predicate selects all pathlines running into the right ventricle during late diastole (see Fig. 6a). Due to the severely incompetent pulmonary valve, the right ventricle receives blood both from the right atrium and the pulmonary trunk. A reduction to lines running through the previously introduced vortices in the bulges of the pulmonary trunk during systole is shown in Fig. 6b. Here, a closer look allows qualitative observations like, e.g., that the vortices in the bulges are mainly avoided by the retrograde blood flow.

The retrograde flow hinders inflow from the right atrium and thus influences the flow behavior in the right atrium in terms of higher residence times. In Fig. 6c, blood particles are shown, which reside in the right atrium for more than $550\ \mathrm{ms}$, i.e., almost the complete cardiac cycle. The same predicate applied to the healthy heart data set shows no results. This indicates that the blood fraction leaving the right atrium is reduced in the TOF patient when compared to the healthy case. To sum up, the analysis of the healthy data set showed that it is feasible to visualize the main phases of the cardiac cycle and that interesting aspects can be extracted. In the pathological cardiac flow, irregularities and hypothesis for their cause could be identified that could not be easily detected with current analysis methods.

5.2.3 Performance

Selection and combination of the line predicates as well as setting the parameters is done interactively. The predicate evaluation time depends on the predicate type and the number of lines. For average cases as shown in Figs. 4, 5, 6a, and 6b, the evaluation takes less than $100\ \mathrm{ms}$ on a standard PC. A more expensive predicate, such as the residence time predicate, takes about $500\ \mathrm{ms}$, when evaluated on a full set of pathlines (as shown in Fig. 6c). The combination of several predicates does not have a significant effect on evaluation time as the number of evaluated lines decreases for each subsequent predicate. The complete update time, i.e., the time needed for predicate evaluation and scene update, is on average below $1\ \mathrm{s}$. This increases of course with the number of rendered lines, but does not exceed $5\ \mathrm{s}$ for a full set of pathlines. This lag could be altogether reduced with an implementation using the GPU more extensively, but in the current version a comfortable line analysis is well possible (see also the supplemental video, which can be found on the Computer Society Digital Library at http://doi.ieeecomputersociety.org/10.1109/TVCG.2012.318).

5.3 Summary of Expert Feedback

The feedback of the three 4D MRI experts (one medical physicist, two radiologists; two are coauthors) showed that our new method provides a yet unknown view on the cardiac blood flow data. The experts rated our approach as well suited to supplement their current analysis techniques in principle, but also commented on drawbacks. In the following, we summarize the experts' feedback in terms of the mentioned advantages, the benefits of the different line predicates, and their suggestions for improvement.

5.3.1 Advantages

One of the advantages that were highly valued by the radiologists, is the global view at the data. Instead of examining local flow features, e.g., on 2D cross-sections, they can inspect various large-scale features and by that identify correlations and causal relationships, which is not possible with state-of-the-art methods (see Section 5.2 for examples). They considered the overview as very important since this allows to exploit the advantage of 4D MRI over 2D cine data (where only local data is acquired). Together

with the reliable and partially automated in vivo identification of secondary flow patterns (vortices), they expect a better understanding of the flow, new insights about flow structures correlating with certain pathologies, and by that about the mechanisms of disease development and maybe also how to improve surgical procedures.

The 4D MRI experts suggested specific research questions where our method could bring a benefit. One such research topic is atrial fibrillation, as it is not yet totally understood why this disease oftentimes correlates with a high risk of blood clot generation that can lead to stroke or heart attack. Further, they were interested in a flow feature analysis with our technique before and after treatment (ablation) of atrial fibrillation with the goal to improve this intervention and to understand the underlying mechanisms.

While current analysis methods mainly rely on the flow interpretation by the user, a standardized flow analysis is necessary for the clinical routine or the more precise evaluation of research studies. The experts considered our method suitable as basis for such a standardized flow analysis by means of predefined line predicate combinations. A more automated approach like this could save time and decrease interobserver variability.

Finally, the experts rated our visualizations as comprehensible and, thus, saw an advantage in using these images in publications.

5.3.2 Benefit of Predicates

The experts' main interests when examining blood flow are—depending on the data set at hand—the velocity distribution, residence times, and irregularities in general. In the following, we describe the usefulness of each of the predicates during flow examination as stated by the experts.

The ROI predicate is useful to allow the examination of the blood flow in or toward a specific area of interest. In most cases, this is applied in combination with other predicates. The length predicate is considered as a supplementary predicate as it is mainly used to reduce clutter.

The velocity predicate is very useful when examining the flow velocity distribution that is one of the medical experts' main interests when it comes to cardiac blood flow. They appreciated the velocity predicate to detect high-velocity flow indicating narrowings (stenosis).

The residence time predicate is better suited to detect blood flowing very slowly or even coming to a halt (see Fig. 6c). It is considered highly useful as very slow flow areas may correlate with a lower heart efficiency (retrograde flow in the TOF data set) and a higher risk for thrombogenesis (blood clot generation).

The vortex predicate was of special interest for the experts, as irregular vortices are a strong indicator for a pathology or for a higher risk for aneurysm development. Our vortex detection in combination with the vortex predicates allow to analyze vortices more systematically. This was rated as a big advantage by the experts, as they have no possibility for vortex analysis right now—except the visual observation of integral lines.

5.3.3 Disadvantages and Improvements

A drawback of our method is the necessary preprocessing time. The experts tolerate about 1 h of preprocessing, which we do not reach yet mainly due to the segmentation overhead. Interestingly, the experts did not claim for a fully automated segmentation approach. Instead, they prefer methods allowing them to interact and apply their medical knowledge to adapt the segmentation.

Another limitation concerns the analysis of smaller flow structures, such as around the valves. Here, it is not yet possible to reliably determine whether blood is flowing through opened or leaky valves or whether integral lines are wrongly crossing the closed valves. These inaccuracies are caused by noise and partial volume effects. Our regional velocity predicate deals with this effect in the sense that one can still evaluate lines in a specific area although it leaks into neighboring chambers. Apart from that, the flow structures detectable with our approach depend mainly on the data quality. Thus, our approach will also benefit from the continuing development of the 4D MRI technique.

In the clinical routine as well as in the medical research, conclusions are preferably drawn based on quantitative parameters like flow rate or blood velocity, instead of qualitative observations. The 4D MRI experts view our method as a valuable supplement to their methods at hand. It would be even more valuable with a quantification of the detected flow features, as this would, e.g., allow the comparison of flow features in healthy and pathological data sets.

Further suggestions are the use of a color-coding convention that is used with, e.g., Doppler-ultrasound, that depicts both flow direction and velocity at the same time. It is thinkable to depict blood flowing from and toward the heart with red and blue respectively.

Concerning the lack of animations in our method, the experts did not agree with each other. On the one hand, it was noted that the neglection of animations is an advantage for a standardized data evaluation and easier to integrate in the clinical and research routine. On the other hand, for the comparison of streamlines of different timesteps an easier way to step through the timesteps was missed.

Finally, as already mentioned before, the experts encouraged us to work toward standardized predicate combinations, which can be used when analyzing larger amounts of data.

6 Discussion and Conclusion

Four-dimensional MRI is a relatively new imaging modality which allows to gain insight into the 3D blood hemodynamics of the cardiovascular system. With that, it has the potential to significantly enhance diagnostics and therapy of cardiovascular diseases. A challenge, however, is to overcome problems in the data analysis that still requires a lot of time and expert knowledge. Physicians have asked for more automated and standardized visualization techniques to open the door for the application of 4D MRI in the clinics or for larger patient studies [21]. This request incorporates methods that are capable of giving the physician a quick overview of the main characteristics and any anomalities of the respective data set. We believe that the development of methods illustrating the overall flow behavior in 3D is an important step toward this goal.

Our approach is based on the fact that the main behavior of a flow field is encoded in its full set of integral lines. To make the flow visualization more comprehensible, we segment these lines into groups of similar behavior. For this grouping, we defined line predicates based on the physicians' needs. They allow to structure integral lines according to certain flow characteristics, such as velocity, anatomical passage areas, and vortices. Users can freely combine these predicates and create flow structures answering their questions about the current data set.

In this paper, we adapted our previously published approach to cardiac 4D MRI blood flow analysis. Here, the challenges are the deformed shape due to the heart beat, the high complexity of the flow, and the lower spatial resolution of the 4D MRI heart data. To cope with them, we adapted the preprocessing, added new features such as the predefinition of meaningful anatomical ROIs, and reshaped and added line predicates.

By means of 4D MRI data sets of a healthy and a pathological heart, we could show that our method allows to easily carve out and display structures of the cardiac flow and to draw conclusions that could not be drawn with other methods presented in literature so far. Three 4D MRI experts gave very positive feedback about our method and stressed the benefit they see for the analysis of 4D MRI data and the medical research on cardiovascular diseases. One limitation is still the preprocessing time that will be reduced in the future by introducing an advanced segmentation approach. Relating to the expert feedback, the goal should be a more sophisticated semiautomated approach with advanced interactive tools for well-trained users in cardiac anatomy.

In addition to this, there are many other interesting topics for future work that were partly suggested by the medical experts. To further improve insight and overview, a reduction of line clutter could be achieved by displaying a line bundle's flow behavior with less lines or more abstract methods. Also, the design of standardized predicate combinations is also an interesting research field. Finally, our visual analysis method helps in gaining overview and understanding the data's overall flow dynamics, but is qualitative so far. We aim to expand our method toward a combined qualitative and quantitative analysis of 4D MRI data.

Acknowledgments

The authors would like to thank Dr. med. Franziska Hause and Dr. med. Emil Ladar for valuable discussions and feedback and Alexander Oeser for his support in preparing the online supplemental material.

References

[1] P. Angelelli and H. Hauser, "Straightening Tubular Flow for Side-by-Side Visualization," *IEEE Trans. Visualization and Computer Graphics,* vol. 17, no. 12, pp. 2063-2070, Dec. 2011.

[2] A. Barker, J. Bock, R. Lorenz, and M. Markl, "4D Flow MR Imaging," *Am. J. Neuroradiology,* vol. 18, pp. 46-52, 2010.

[3] H.G. Bogren and M.H. Buonocore, "4D Magnetic Resonance Velocity Mapping of Blood Flow Patterns in the Aorta in Young vs. Elderly Normal Subjects," *J. Magnetic Resonance Imaging,* vol. 10, no. 5, pp. 861-869, 1999.

[4] S. Born, M. Pfeifle, M. Markl, and G. Scheuermann, "Visual 4D MRI Blood Flow Analysis with Line Predicates," *Proc. IEEE Pacific Visualization Symp.,* pp. 105-112, 2012.

[5] M.H. Buonocore, "Visualizing Blood Flow Patterns Using Streamlines, Arrows, and Particle Paths," *Magnetic Resonance in Medicine,* vol. 40, no. 2, pp. 210-226, 1998.

[6] J.R. Dormand and P.J. Prince, "A Family of Embedded Runge-Kutta Formulae," *J. Computational and Applied Math.,* vol. 6, no. 1, pp. 19-26, 1980.

[7] J. Eriksson, C.J. Carlhäll, P. Dyverfeldt, J. Engvall, A.F. Bolger, and T. Ebbers, "Semi-Automatic Quantification of 4D Left Ventricular Blood Flow," *J. Cardiovascular Magnetic Resonance,* vol. 12, no. 1, p. 9, 2010.

[8] A. Fyrenius, L. Wigstrom, T. Ebbers, M. Karlsson, J. Engvall, and A. Bolger, "Three Dimensional Flow in the Human Left Atrium," *Heart,* vol. 86, no. 4, pp. 448-455, 2001.

[9] R. Gasteiger, M. Neugebauer, C. Kubisch, and B. Preim, "Adapted Surface Visualization of Cerebral Aneurysms with Embedded Blood Flow Information," *Proc. Eurographics Workshop Visual Computing for Biology and Medicine,* pp. 25-32, 2010.

[10] J. Geiger, M. Markl, B. Jung, J. Grohmann, B. Stiller, M. Langer, and R. Arnold, "4D-MR Flow Analysis in Patients After Repair for Tetralogy of Fallot," *European Radiology,* vol. 21, no. 8, pp. 1651-1657, Aug. 2011.

[11] M. Grothoff, B. Spors, H. Abdul-Khaliq, and M. Gutberlet, "Evaluation of Postoperative Pulmonary Regurgitation After Surgical Repair of Tetralogy of Fallot: Comparison between Doppler Echocardiography and MR Velocity Mapping," *Pediatric Radiology,* vol. 38, no. 2, pp. 186-191, 2008.

[12] E. Heiberg, T. Ebbers, L. Wigstrom, and M. Karlsson, "Three-Dimensional Flow Characterization Using Vector Pattern Matching," *IEEE Trans. Visualization and Computer Graphics,* vol. 9, no. 3, pp. 313-319, July-Sept. 2003.

[13] E. Heiberg, J. Sjögren, M. Ugander, M. Carlsson, H. Engblom, and H. Arheden, "Design and Validation of Segment - Freely Available Software for Cardiovascular Image Analysis," *BMC Medical Imaging,* vol. 10, p. 1, 2010.

[14] J. Jeong and F. Hussain, "On the Identification of a Vortex," *J. Fluid Mechanics,* vol. 285, pp. 69-94, 1995.

[15] M. Jiang, R. Machiraju, and D. Thompson, "Detection and Visualization of Vortices," C.D. Hansen and C.R. Johnson, eds., *The Visualization Handbook,* vol. 14, pp. 295-309, Academic Press, 2005.

[16] D. Kainmüller, R. Unterhinninghofen, S. Ley, and R. Dillmann, "Level Set Segmentation of the Heart From 4D Phase Contrast MRI," *Proc. SPIE,* vol. 6914, no. 1, 2008.

[17] P.J. Kilner, G.Z. Yang, R.H. Mohiaddin, D.N. Firmin, and D.B. Longmore, "Helical and Retrograde Secondary Flow Patterns in the Aortic Arch Studied by Three-Directional Magnetic Resonance Velocity Mapping," *Circulation,* vol. 88, pp. 2235-2247, 1993.

[18] P.J. Kilner, G.Z. Yang, A.J. Wilkes, R.H. Mohiaddin, D.N. Firmin, and M.H. Yacoub, "Asymmetric Redirection of Flow through the Heart," *Nature,* vol. 404, no. 6779, pp. 759-761, 2000.

[19] H. Krishnan, C. Garth, J. Guhring, M.A. Gulsun, A. Greiser, and K.I. Joy, "Analysis of Time-Dependent Flow-Sensitive PC-MRI Data," *IEEE Trans. Visualization and Computer Graphics,* vol. 17, no. 11, pp. 1-13, Apr. 2011.

[20] M. Markl, F.P. Chan, M.T. Alley, K.L. Wedding, M.T. Draney, C.J. Elkins, D.W. Parker, R. Wicker, C.A. Taylor, R.J. Herfkens, and N.J. Pelc, "Time-Resolved Three-Dimensional Phase-Contrast MRI," *J. Magnetic Resonance Imaging,* vol. 17, no. 4, pp. 499-506, 2003.

[21] M. Markl, P.J. Kilner, and T. Ebbers, "Comprehensive 4D Velocity Mapping of the Heart and Great Vessels by Cardiovascular Magnetic Resonance," *J. Cardiovascular Magnetic Resonance,* vol. 13, no. 7, 2011.

[22] M. Neugebauer, G. Janiga, O. Beuing, M. Skalej, and B. Preim, "Anatomy-Guided Multi-Level Exploration of Blood Flow in Cerebral Aneurysms," *Computer Graphics Forum,* vol. 30, no. 3, pp. 1041-1050, 2011.

[23] R. Peikert and M. Roth, "The Parallel Vectors Operator: A Vector Field Visualization Primitive," *Proc. IEEE Visualization Conf.,* pp. 263-270, 1999.

[24] A. Pobitzer, A. Lez, K. Matkovic, and H. Hauser, "A Statistics-Based Dimension Reduction of the Space of Path Line Attributes for Interactive Visual Flow Analysis," *Proc. IEEE Pacific Visualization Symp.,* pp. 113-120, 2012.

[25] P. Rautek, S. Bruckner, and E. Gröller, "Semantic Layers for Illustrative Volume Rendering," *IEEE Trans. Visualization and Computer Graphics,* vol. 13, no. 6, pp. 1336-1343, Nov. 2007.
[26] T. Salzbrunn, C. Garth, G. Scheuermann, and J. Meyer, "Pathline Predicates and Unsteady Flow Structures," *Visual Computer,* vol. 24, no. 12, pp. 1039-1051, 2008.
[27] T. Salzbrunn and G. Scheuermann, "Streamline Predicates," *IEEE Trans. Visualization and Computer Graphics,* vol. 12, no. 6, pp. 1601-1612, Nov./Dec. 2006.
[28] K. Shi, H. Theisel, H. Hauser, T. Weinkauf, K. Matkovic, H.-C. Hege, and H.P. Seidel, "Path Line Attributes - An Information Visualization Approach to Analyzing the Dynamic Behavior of 3D Time-Dependent Flow Fields," *Proc. TopoInVis Conf.,* pp. 75-88, 2009.
[29] S. Silva, B. Sousa Santos, and J. Madeira, "Using Color in Visualization: A Survey," *Computer and Graphics,* vol. 35, no. 2, pp. 320-333, 2011.
[30] D. Silver and X. Wang, "Volume Tracking," *Proc. Seventh Conf. Visualization,* pp. 157-164, 1996.
[31] D. Sujudi and R. Haimes, "Identification of Swirling Flow in 3D Vector Fields," technical report AIAA Paper 95-1715, Am. Inst. of Aeronautics and Astronautics, 1995.
[32] R. van Pelt, J.O. Bescós, M. Breeuwer, R.E. Clough, M.E. Gröller, B.T.H. Romenij, and A. Vilanova, "Interactive Virtual Probing of 4D MRI Blood-Flow," *IEEE Trans. Visualization and Computer Graphics,* vol. 17, no. 12 pp. 2153-2162, Dec. 2011.
[33] R. van Pelt, H. Nguyen, B. ter Haar Romeny, and A. Vilanova, "Automated Segmentation of Blood-Flow Regions in Large Thoracic Arteries Using 3D-Cine PC-MRI Measurements," *Int'l J. Computer Assisted Radiology Surgery,* vol. 2, pp. 217-224, 2011.
[34] R. van Pelt, J. Oliván Bescós, M. Breeuwer, R.E. Clough, M.E. Gröller, B. ter Haar Romeny, and A. Vilanova, "Exploration of 4D MRI Blood-Flow Using Stylistic Visualization," *IEEE Trans. Visualization and Computer Graphics,* vol. 16, no. 6, pp. 1339-1347, Nov./Dec. 2010.
[35] R.F.P. van Pelt, S.S.a.M. Jacobs, B.M. ter Haar Romeny, and A. Vilanova, "Visualization of 4D Blood-Flow Fields by Spatiotemporal Hierarchical Clustering," *Computer Graphics Forum,* vol. 31, pp. 1065-1074, June 2012.
[36] P.G. Walker, G.B. Cranney, M.B. Scheidegger, G. Waseleski, G.M. Pohost, and A.P. Yoganathan, "Semiautomated Method for Noise Reduction and Background Phase Error Correction in Mr Phase Velocity Data," *J. Magnetic Resonance Imaging,* vol. 3, no. 3, pp. 521-530, 1993.
[37] S. Zachow, P. Muigg, T. Hildebrandt, H. Doleisch, and H.-C. Hege, "Visual Exploration of Nasal Airflow," *IEEE Trans. Visualization and Computer Graphics,* vol. 15, no. 6, pp. 1407-1414, Nov./Dec. 2009.

Silvia Born received the MS degree (diplom) in computer science (bioinformatics) from the University of Tübingen in 2007. Currently, she is a research assistant at the Medical Faculty of the University of Leipzig and associated researcher at the Department for Computer Science at the same university. Her research interests include illustrative rendering techniques and medical visualization with focus on medical flow visualization.

Matthias Pfeifle received the MS degree (diplom) in computer science from the University of Tübingen where he studied bioinformatics with focus on neurobiology. He is a research assistant at the Neurosurgical Department of the University of Tübingen. During his studies, he worked in the field of medical visualization at GRIS of the University of Tübingen. His research interests include medical image visualization and medical augmented reality.

Michael Markl received the PhD degree in physics at the University of Freiburg, Germany, in 2000. He is an associate professor of radiology and biomedical engineering and the director of cardiovascular MRI research in the Department of Radiology at Northwestern University. After working at the Lucas MRI/S Center at Stanford University as a postdoctoral fellow and research associate (2001-2004), he returned to University Hospital in Freiburg, Germany, as the director of cardiovascular MRI. From 2007-2010, he was the deputy director of the Freiburg Medical Physics group. His research interests include the field of cardiovascular MR imaging. The work of his research group has been instrumental in establishing "4D Flow" MR imaging methods and data analysis tools for the comprehensive assessment of 3D blood flow and cardiovascular function. The evaluation of such methods in clinical studies and translation into novel clinical applications represent important aspects of past and ongoing scientific activities.

Matthias Gutberlet is a professor of radiology and chair of the Department of Diagnostic and Interventional Radiology of the University of Leipzig, Leipzig Heart Center, since 2007. From 2002, he was associate professor at the Charité in Berlin working on the use of Cardiac MRI and MR flow measurements on patients with congenital heart disease. He is also one of the principle investigators of Cardiac MRI in the German Competence Network for Congenital Heart Defects. Beside the use of 2D and 4D flow measurements of the heart and its great vessels, his recent research interests include all kinds of noninvasive cardiovascular imaging (MRI, MDCT, SPECT, and PET/MRI) as well as interventional MRI in patients after acute myocardial infarction, suspected coronary artery disease, arrhythmias, cardiomyopathies, and myocarditis.

Gerik Scheuermann received the PhD degree in computer science from the University of Kaiserslautern in 1999. From 1995-1997, he conducted research at Arizona State University. He worked as a postdoctoral researcher at the Center for Image Processing and Integrated Computing at the University of California, Davis, in 1999 and 2000. Between 2001 and 2004, he was an assistant professor for computer science at the University of Kaiserslautern. He is currently a full professor in the Computer Science Department of the University of Leipzig. His research interests include topology, Clifford algebra, image processing, visualization, and visual analytics. He is a member of the IEEE and GI.